Cecconi A, Vilchez-Tschischke JP, Mateo J, Sanchez-Gonzalez J, Espana S, Fernandez-Jimenez R, Lopez-Melgar B, Fernandez Friera L, Lopez-Martin GJ, Fuster V, Ruiz-Cabello J, Ibanez B. (2021). Effects of Colchicine on Atherosclerotic Plaque Stabilization: a Multimodality Imaging Study in an Animal Model. *J Cardiovasc Transl Res*, 14(1), 150-60. doi: 10.1007/s12265-020-09974-7

Effects of Colchicine on Atherosclerotic Plaque Stabilization: a Multi-modality Imaging Study in an Animal Model.

Alberto Cecconi MD PhD [1,2,#], Jean Paul Vilchez-Tschischke MD[1,3,#], Jesus Mateo PhD[1], Javier Sanchez-Gonzalez PhD[4], Samuel España PhD[1], Rodrigo Fernandez-Jimenez MD PhD [1,5,6], Beatriz Lopez-Melgar MD PhD [1,6,7], Leticia Fernández Friera MD PhD [1,6,8], Gonzalo J López-Martín PhD[1], Valentin Fuster MD PhD[1,5], Jesus Ruiz-Cabello PhD[9] and Borja Ibañez MD PhD[1,6,10]

[#] both authors equally participated in the manuscript

[1] Centro Nacional de Investigaciones Cardiovasculares (CNIC), Madrid, Spain.

[2] Servicio de Cardiología, Hospital Universitario de La Princesa, Madrid, Spain

[3] Servicio de Cardiología, Complejo hospitalario Ruber Juan Bravo, Madrid, Spain

[4] Philips Healthcare, Madrid, Spain

[5] The Zena and Michael A. Wiener Cardiovascular Institute, Icahn School of Medicine at Mount Sinai, New York, USA

[6] CIBER de Enfermedades Cardiovasculares (CIBERCV), Madrid, Spain

[7] Servicio de Cardiología, Hospital Universitario HM Puerta del Sur, Móstoles, Spain

[8] HM Hospitales-Centro Integral de Enfermedades Cardiovasculares HM-CIEC, Madrid, Spain.

[9] CIC biomaGUNE, 2014, Donostia-San Sebastián, Spain; IKERBASQUE, Basque Foundation for Science, Spain; CIBER de Enfermedades Respiratorias (CIBERES), Madrid, Spain; and Universidad Complutense Madrid, Madrid, Spain.

[10] Servicio de Cardiología, IIS-Fundación Jiménez Díaz Hospital, Madrid, Spain.

Total word count: 5901

Address for correspondence:

Borja Ibanez, MD PhD FESC. Centro Nacional de Investigaciones Cardiovasculares (CNIC), Calle de Melchor Fernández Almagro, 3, 28029, Madrid, Spain.

Tel: +34 914531200 (ext 4302). Fax: +34 915202201. Email: bibanez@cnic.es

Abbreviations:

^{18}F-FDG PET/CT, ^{18}F-Fluorodeoxyglucose Integrated with Computed Tomography;

MRI, Magnetic Resonance Imaging;

NWI, Normalized Wall Index;

OCT, Optical Coherence Tomography;

SUV, Standardized Uptake Values.

Abstract:

Colchicine demonstrated clinical benefits in the treatment of stable coronary artery disease. Our aim was to evaluate the effects of colchicine on atherosclerotic plaque stabilization. Atherosclerosis was induced in the abdominal aorta of 20 rabbits with high-cholesterol diet and balloon endothelial denudation. Rabbits were randomized to receive either colchicine or placebo. All animals underwent MRI, ^{18}F-FDG PET/CT, OCT and histology.

Similar progression of atherosclerotic burden was observed in the two groups as relative increase of normalized wall index (NWI). Maximum ^{18}F-FDG standardized uptake value (meanSUVmax) decreased after colchicine treatment, while it increased in the placebo group with a trend toward significance. Animals with higher levels of cholesterol showed significant differences in favor to colchicine group, both as NWI at the end of the protocol and as relative increase in meanSUVmax.

Colchicine may stabilize atherosclerotic plaque by reducing inflammatory activity and plaque burden, without altering macrophage infiltration or plaque typology.

Keywords: Imaging, Atherosclerosis, Animal Model, Colchicine, Inflammation, Plaque morphology.

Introduction:

Atherosclerosis is characterized by a chronic inflammatory activity [1, 2]. Recruitment of leucocytes within the vascular wall occurs in an early stage of the atherosclerotic plaque formation and their consecutive activation produces pro-inflammatory cytokines and matrix metalloproteinases that promote the process by degrading the extracellular matrix [3, 4]. Observational studies support the relevant role of inflammation**,** since systemic inflammatory diseases or high levels of C-reactive protein are well known cardiovascular risk factors [5, 6]. Moreover, beneficial effects of statins are related to an anti-inflammatory action in parallel to their main effects as cholesterol-lowering drugs [7]. Furthermore, a recent randomized clinical trial showed that modulation of innate immunity pathway reduces recurrent cardiovascular events, independent of lipid-level lowering [8]. For all these reasons, interest in the anti-inflammatory treatment of atherosclerosis is an expanding field of research [8-10].

Colchicine is an alkaloid extracted from *Colchicum autumnale* and is one of the drugs under investigation for the treatment of atherosclerotic disease [11]. Initially, a beneficial effect on atherosclerosis has been suggested by retrospective observations, since continuous use of colchicine in patients with gout or familiar mediterranean fever was associated with a reduction of myocardial infarctions [12, 13]. In the Low-Dose-Colchicine (LoDoCo) pilot trial -a prospective, randomized, observer blinded endpoint study- colchicine added to standard therapy of secondary prevention in patients with stable coronary artery disease, reduced the incidence of acute coronary syndrome [14]. The LoDoCo 2 –a double-blind, event driven trial including 5522 patients- is currently ongoing [15]. In addition, colchicine has been associated with less neointimal hyperplasia in diabetic patients after percutaneous coronary interventions with bare metal stents [16]. Finally, the COLCOT trial – a randomized, double-blind study- showed that colchicine led to a significantly lower risk of ischemic cardiovascular events than placebo among patients with a recent myocardial infarction[17].

Although basic research has demonstrated several cellular mechanisms of colchicine related to its anti-inflammatory effect [18-25], the mechanism by which this substance might stabilize the atherosclerotic plaque *in vivo* still remains unclear. The present study was designed to assess the effect of colchicine treatment on plaque progression, plaque composition and vessel wall inflammation in an experimental model of atherosclerosis. To reach our aim we used the established rabbit model and performed a comprehensive serial imaging study including magnetic resonance imaging (MRI), positron emission tomography with ^{18}F-fluorodeoxyglucose integrated with computed tomography (^{18}F-FDG PET/CT), ex-vivo optical coherence tomography (OCT) and histology.

Methods:

Experimental Design:

The experimental scheme is shown in Figure 1. Aortic atherosclerosis was induced in New Zealand White male rabbits (n=20; mean age 3 months; 3.1±0.3 kg; Charles River, L'arbresle Cedex, France). The study protocol lasted 36 weeks. Animals were fed an atherogenic diet containing 0.2% cholesterol (LabDiet 5322, 0.2% cholesterol, TestDiet®, London, UK) during the entire duration of the study. Balloon endothelial denudation of the abdominal aorta was performed two weeks after high cholesterol diet initiation using 3-4F Fogarty catheters introduced through a femoral access. This atherogenic protocol has been fully described previously [26]. After 18 weeks animals were randomized into two groups to receive either colchicine at 0.2 mg/kg/day, 5 days/week, subcutaneously (Colchicine C3915, Sigma-Aldrich, Missouri, USA) or placebo (saline solution, 1 ml/day, 5 days/week, subcutaneously), and were followed up for another 18 weeks. Colchicine was reconstructed in sterile water (5mg/ml) using laminar air flow cabinet. Before randomization and at the end of the study, all animals underwent MRI and ^{18}F-FDG PET/CT of the abdominal aorta. Animals were euthanized with an overdose of pentobarbital. Immediately after sacrifice, the aortas were imaged by optical coherence tomography. Thereafter, the abdominal aortas were harvested and processed for histological analysis. For all techniques, the right renal artery served as the anatomical reference marker and the analysis focused on 8-cm of aorta around it (Figure 2). This study was conducted according to the guidelines of the current European Directive and Spanish legislation and approved by the regional ethical committee for animal experimentation.

Magnetic Resonance Imaging:

Prior to imaging, the animals were anesthetized by intramuscular injection of ketamine (10 mg/kg) and xylazine (5 mg/kg). Anesthesia was maintained during the MRI sessions with isoflurane inhalation (1.2-1.5%) via a facemask. MR images were collected with a 3 Tesla MRI system (Philips Health Care, Andover, MA, USA) and a conventional knee coil. We obtained 40 sequential axial slices, 2-mm thick, with no gap, using a T2-weighted (TR/TE 2300/62 ms) and T1-weighted fast spin echo (resolution 0,4 x 0,4 mm; TR/TE 1000/15 ms) sequence for each aorta. An observer blinded to treatment allocation traced the aortic lumen and outer wall. Plaque volume burden was assessed as the sum of vessel wall area of each slice (outer wall area minus lumen area) as described elsewhere [27]. Results were expressed as Normalized Wall Index (NWI), derived as aortic wall volume divided by the total vessel volume.

^{18}F-FDG PET/CT Imaging:

^{18}F-FDG PET images were acquired in fasting animals 3-hours after the intravenous injection of 111-148 MBq [3-4 mCi (~1 mCi/kg)] of ^{18}F-FDG, using a combined PET/CT scanner (Gemini TF 64, Philips Medical Systems). Prior to imaging, the animals were anesthetized with ketamine/xylazine as described before and placed in prone position in a dedicated animal support on top of the scanner bed. A non-contrast low-dose CT scan was obtained (120 kV, 200 mA, 0.5 s rotation time, 64 × 0.625 mm collimation, pitch of 0.703, 2.0 mm slice thickness) before the PET scan for anatomic registration and for attenuation correction of the PET dataset. PET imaging of the entire aorta was acquired including 3 bed positions with 50% bed overlapping (5 minutes per bed) in order to ensure a uniform sensitivity across the region of interest. The resulting images were reconstructed using the scanner implemented LOR-RAMLA algorithm. The final image matrix contained 174 slices of 128 x 128 voxels, with 2.0 x 2.0 x 2.0 mm voxel size, using corrections for normalization, dead time, attenuation, scatter, random coincidences, sensitivity and decay.

For PET image analysis, circular regions of interest (ROIs) encompassing the vessel wall were manually drawn on the corresponding axial CT images covering the 8-cm stretch of abdominal aorta and centered at the right renal artery using OsiriX Imaging Software (Pixmeo, Geneva, Switzerland). ROIs were quantified using the standardized uptake values (SUV). Maximum SUV were obtained in each ROI and averaged across the entire artery (meanSUVmax) for each PET scan. In addition, high intensity CT plaque volume was measured as the volume within the ROI with HU greater than 65 and results were expressed as high intensity plaque volume (mm^3) per animal [28] .

Optical Coherence Tomography:

Immediately after animal sacrifice, the thoracic aorta was cannulated with two 16-Gauge catheters. An OCT imaging catheter (Dragonfly™ OPTIS™, St. Jude Medical, Minnesota, USA) was then inserted through one of the access down to the abdominal aorta. Since the blood is highly scattering for light, blood clearance was performed with continuous saline infusion through the remaining access. Finally, aorta was scanned with sequences of optical coherence tomography automatic pullbacks. After localizing the right renal artery as the middle point, 80 sequential axial slices, with 1-mm gap, were analyzed for each aorta. Quadrants of aortic vessel were classified as normal wall, fibrotic plaque or lipid plaque.

Minimum fibrous cap was measured for each slice. Results were expressed as the percentage of lipid plaque and average of minimum fibrous cap per animal.

Histology and Immunostaining:

Following the OCT imaging session, the aorta was perfused with phosphate-buffered saline, gently removed, and fixed in 10% buffered-formalin. The 8-cm stretch under study was cut into 4-mm segments, tagged for orientation, and embedded in paraffin. Serial sections (4-µm thick) were obtained and stained with hematoxylin-eosin. Macrophages were identified on adjacent slices using a mouse monoclonal antibody directed against RAM-11, a marker of rabbit macrophage cytoplasm (1:1000 dilution, Dako). In a post-hoc assessment, smooth muscle cells were stained using a smooth muscle actin antibody (1:500 dilution, Sigma). Results were expressed as percentage of total vessel wall area occupied by macrophages and smooth muscle cells per animal.

Plasma Analysis:

Blood samples from all animals were drawn at fasting condition from the marginal ear-vein and collected in EDTA tubes at time of randomization and previous to sacrifice. Blood samples were centrifuged (2000 x *g* for 20 min at 4°C) and plasma was stored in aliquots at -80°C until analysis. Lipid profiles were assessed. In addition, in a post-hoc analysis interleukin 6 (IL-6) was assessed in the samples collected at the end of the protocol using a commercial ELISA kit (Elabscience).

Statistical Analysis:

All data are presented as medians and interquartile range (IQR). Statistical comparisons were made by using the Mann–Whitney U test for unpaired data and Wilcoxon signed-rank test for paired data; probability values of <0.05 were considered statistically significant. Initially the analysis was performed including all animals, thereafter a *post-hoc* subgroup analysis was performed after excluding animals of each group in the first quartile of cholesterol levels. Confidence intervals were calculated by Hodges-Lehmann's estimator. All analyses were performed with SPSS statistics 23.0 and GraphPad Prism 5.

Results:

Animal characteristics and lipid profile.

At 18 and 36 weeks the atherogenic diet was associated with severe dyslipidemia in both groups. There were no significant differences between the two groups in total cholesterol, LDL-cholesterol, HDL-cholesterol, or body weight throughout the course of the study (Table 1). Two rabbits died during the first 18 weeks atherosclerosis induction phase (i.e. before randomization) secondary to vascular complications of arterial access for the denudation procedure, while two rabbits (one in colchicine and one in control groups) died between weeks 18 and 36 .

Imaging assessment’s results are summarized in Table 2.

Plaque burden analysis. During the treatment phase, NWI increased significantly in both groups. Relative increase of NWI [12.0% (IQR 10.0%) in colchicine group versus 14.4 % (IQR 10.1%) in placebo; p = 0.33] showed no differences in plaque progression (Figure 3). Neither aortic wall area occupied by smooth muscle cell showed any significant difference [13.0% (IQR 9.9 %) in colchicine group versus 8.7% (IQR 5.5 %) in placebo; p = 0.20].

Inflammation analysis. ^{18}F-FDG uptake of the abdominal aorta decreased in the colchicine group, while it increased in the placebo group with a trend towards significance [-10.9% mean SUVs (IQR 32.1%) in colchicine group versus +13.7% (IQR 48.6%) in placebo; p = 0.13] (Figure 4). In accordance with the uptake of ^{18}F-FDG, we observed a slight but non-significant reduction in the aortic wall area occupied by macrophages by immunostaining with RAM-11 [16.6% (IQR 19.2%) in colchicine group versus 24.0 % (IQR

31.1%) in placebo; p = 0.77)]. Similarly, at the end of the study a favorable non-significant lower concentration of IL-6 was detected [75 pg/mL (IQR 865 pg/mL) in the colchicine group versus 377 pg/mL (IQR 756 pg/mL) in placebo; p = 0.20).

Plaque typology. The analysis of the aortas by OCT showed no differences neither in the typology of atherosclerotic plaques (94% of lipid plaque in colchicine group versus 93% in placebo; p = 0.88) nor in the minimum fibrous cap [119.1 µm (IQR 37.1 µm) in colchicine group versus 113.0 µm (IQR 24.5 µm) in placebo; p = 0.88]. The quantification of high CT-intensity plaque volume increased in both groups, but no differences were observed as absolute increase [12.08 mm^3 (IQR 13.94 mm^3) in colchicine group versus 10.63 mm^3 (IQR 32.19 mm^3) in placebo; p = 0.96]. See Figure 5.

Subgroup analysis in animals with higher cholesterol levels. In this post-hoc analysis, animals in the colchicine and placebo subgroups did not show any difference in body weight during the study and IL-6. Six animals per group were selected (lower quartile was excluded). Significant differences in favor of colchicine were found both as NWI at the end of the protocol [0.47 (IQR 0.05) in the colchicine group versus 0.52 (IQR 0.03) in the placebo; p = 0.01] and as relative decrease of uptake of ^{18}F-FDG during the protocol [-4.0% (IQR 30.1%) in the colchicine group versus 35.1 % (IQR 59.0%) in the placebo; p 0.041] (Figure 6). There were no differences in the other morphological variables of the study (Table 3). In addition, HDL was higher in the colchicine group at the end of the protocol [198 mg/dl (IQR 61 mg/dl) in the colchicine group versus 151 mg/dl (IQR 41 mg/dl) in the placebo; p 0.041], but no other differences were found in the remaining lipid profile.

Discussion:

In patients with stable coronary artery disease colchicine has shown promising effects in the secondary prevention of coronary ischemic events [14]. However, the mechanisms by which this drug could modulate the atherosclerotic process *in vivo* are unknown. This is the first study using non-invasive imaging to assess atherosclerosis progression in an animal model under colchicine treatment and to provide a complete *in vivo* multimodality imaging of atherosclerosis with a combination of MRI, ^{18}F-FDG PET, OCT and immunohistology.

The term “vulnerable plaque” is used to define plaques susceptible to generate thrombotic complications. Classically, a large lipid-rich core with a thin fibrous cap infiltrated by macrophages, an expansive remodeling and a large plaque size are the common morphologic features proposed for detection of vulnerable plaques [29]. However, despite the ability to identify atherosclerotic lesions that exhibit these vulnerable characteristics, clinical studies have failed to demonstrate meaningful utility of individual plaque imaging [30]. Recent publications about vulnerability reiterated the importance of going beyond a vulnerable individual plaque and called for evaluating the total arterial tree as a whole [31]. This suggests that detection of a *state* of vulnerability in a patient is more important than detection of individual *sites* of vulnerability [32]. Accordingly, the strongest predictors of adverse events are the plaque burden and inflammatory activity of the whole coronary artery bed.

NWI estimated by MRI is a validated approach for the quantification of plaque burden and is good indicator of future coronary events [33, 34]. In the main analysis of our study, NWI showed atherosclerotic progression with no significant differences between the two groups, however subgroup analysis in animals with higher cholesterol levels showed a smaller NWI in the colchicine subgroup at the end of the protocol. These findings may be related with the results of a recent observational study that showed a reduction of low attenuation plaque volume assessed by CT imaging in patients treated with colchicine after an acute coronary syndrome [35]. Considering that the inhibition of smooth muscle cell proliferation by colchicine [36] might partially explain the observed difference of NWI in the animal subgroup with higher levels of cholesterol, we performed a post-hoc analyses to explore this hypothesis. However, we found no differences in area occupied by smooth muscle cell neither in main analysis nor in subgroup analysis.

Inflammatory activity within the atherosclerotic vessel expresses an active disease with higher risk of complications. This activity can be demonstrated by ^{18}F-FDG PET imaging *in vivo* and by macrophage infiltration *ex vivo* [37, 38]. In addition, it has been proven that the response to cardiovascular drugs can be assessed by monitoring the change of ^{18}F-FDG uptake [39, 40]. Noteworthy, in the main analysis of this study we observed a divergent trend of inflammatory activity in favor of the colchicine group, measured by ^{18}F-FDG PET uptake, that became statistically significant in the subgroup analysis excluding animals with lower level of cholesterol. Cholesterol crystals have been recently related to the activation of the NLRP3 inflammasome producing the inflammatory cascade that drives the progression of atherosclerosis process [41]. Since colchicine has demonstrated to inhibit the activation of NLRP3 inflammasome by cholesterol crystal, it is intriguing to speculate that the observed benefit in animals with higher cholesterol levels might be related to a higher amount of cholesterol crystal and a consequently inhibition by colchicine of this inflammatory pathway in this subgroup. Further studies should confirm this hypothesis.

On the other hand, histological density of macrophages assessed by RAM-11 staining showed slight differences with lack of statistical significance. This discrepancy between macrophage activity and macrophage infiltration might be explained by the limitation of the animal model. The traumatic effect of balloon injury, previous to the colchicine treatment, may have negatively influenced the macrophage infiltration. In no-traumatic atherosclerosis, as in human process, colchicine could have a more relevant effect on endothelial permeability to leukocytes than what we documented in our study. In patients presenting with acute coronary syndrome the acute administration of colchicine reduces the production of IL-6 [42]. Consistent with this previous report, in a post-hoc analysis, we observed lower values of IL-6 in the colchicine group. This difference was not statistically significant, however, the lack of data about IL-6 at randomization, did not allow us to explore the change of IL-6 in response to colchicine.

Intravascular OCT provides high-resolution cross-sectional images of tissue *in situ* and allows plaque characterization *in vivo* [43]. *In vitro* studies have proposed a fibrous cap less than 65 µm thick as a criterion of vulnerable plaque. Nevertheless, this threshold may be higher when assessed *in vivo* because histologic fixation implies dehydration processes [44]. In our study, no differences were observed in both groups in terms of lipid plaque proportion and mean minimum fibrous cap. Nonetheless, our results confirm this animal model as a valid model for the study of coronary atherosclerosis. Indeed, a high prevalence of lipid plaques with luminal area and mean fibrous cap similar to *in vivo* human atherosclerotic coronary disease was detected.

High intensity CT plaque volume showed no difference between the two groups. However, the usefulness of CT to monitor the changes of vascular risk in response to pharmacological treatment is controversial, since this technique cannot differentiate the fibrocalcific proportion of atherosclerotic plaque secondary to the progression of the disease from that secondary to the stabilization of the atherosclerotic process [45].

Our study has several limitations. In clinical trials using colchicine among patients with coronary artery disease it has been administrated a daily oral low dose of 0.5-1 mg [14, 16, 17]. In translational experiments, according to the animal model and the therapeutic purposes investigated, different doses and routes of administration (transdermal, subcutaneous, intramuscular, oral, intraperitoneal and intravenous) have been used [46-50]. Oral administration of colchicine is associated with gastrointestinal side effects [51] leading to limited drug tolerance and absorption. Consequently, looking for a balance among comfort for the animals, tolerance of the administration and working schedule of our laboratory, we selected the subcutaneous injections for 5 days a week as our route of administration. Further studies should explore the most effective dose and route of administration.

Nowadays treatment of coronary artery disease follows a poly-drug scheme with a synergic effect on the disease, but our study was developed in a mono-drug scenario. This could have limited the effect of colchicine compared with the one observed in clinical trials. Although we have observed beneficial trends in ^{18}F-FDG uptake and slight difference in the amount of infiltrated macrophages none reached the significance threshold in the main analysis; this could be partially explained by the high variability of dyslipidemia in response to the atherogenic diet. As observed in our study, the response to atherogenic diet may vary markedly among rabbits in this animal model. Since dyslipidemia is the major proatherosclerotic factor of this model, the high variance of cholesterol levels may significantly reduce the activity of atherosclerosis in the animals with low level of cholesterol and, therefore, the observed response to colchicine. For this reason, we considered mandatory to include a not pre-specified subgroup analysis focusing on the animals with higher levels of cholesterol.

In conclusion, and given the limitations discussed above, our study suggests that colchicine, *in vivo*, could reduce vulnerability state of coronary artery disease by a reduction of inflammatory activity and plaque burden, instead of plaque typology or leucocytes infiltration.

Compliance with Ethical Standards:

Funding**:** *This work was supported by a grant from the Sociedad Española de Cardiología, a grant from the Carlos III Institute of Health of Spain and Fondo Europeo de Desarrollo Regional (FEDER, "Una manera de hacer Europa") (FIS-FEDER PI14-01427 to J. Mateo) and from a grant from Fundación BBVA to J. Ruiz-Cabello. The CNIC is supported by the Ministry of Science, Innovation and Universities (MICIN) and the Pro CNIC Foundation, and is a Severo Ochoa Center of Excellence (SEV-2015-0505). CIC biomaGUNE is supported* *by the Spanish State Research Agency of MICIN under the María de Maeztu Units of Excellence Program from (MDM-2017-0720).*

Ethical approval: This article does not contain any studies with human participants performed by any of the authors.

All institutional and national guidelines for the care and use of laboratory animals were followed and approved by the appropriate institutional committees

Conflicts of interest: none.

References:

1. Tousoulis, D., et al., *Inflammatory cytokines in atherosclerosis: current therapeutic approaches.* Eur Heart J, 2016. **37**(22): p. 1723-32.
2. Libby, P., *Inflammation in atherosclerosis.* Arterioscler Thromb Vasc Biol, 2012. **32**(9): p. 2045-51.
3. Naruko, T., et al., *Neutrophil infiltration of culprit lesions in acute coronary syndromes.* Circulation, 2002. **106**(23): p. 2894-900.
4. Vacek, T.P., et al., *Matrix metalloproteinases in atherosclerosis: role of nitric oxide, hydrogen sulfide, homocysteine, and polymorphisms.* Vasc Health Risk Manag, 2015. **11**: p. 173-83.
5. Peters, M.J., et al., *Does rheumatoid arthritis equal diabetes mellitus as an independent risk factor for cardiovascular disease? A prospective study.* Arthritis Rheum, 2009. **61**(11): p. 1571-9.

6. Ridker, P.M., *Inflammation, C-reactive protein, and cardiovascular disease: moving past the marker versus mediator debate.* Circ Res, 2014. **114**(4): p. 594-5.

7. Moreno, P.R. and A. Kini, *Resolution of inflammation, statins, and plaque regression.* JACC Cardiovasc Imaging, 2012. **5**(2): p. 178-81.

8. Ridker, P.M., et al., *Antiinflammatory Therapy with Canakinumab for Atherosclerotic Disease.* N Engl J Med, 2017. **377**(12): p. 1119-1131.

9. Ridker, P.M., et al., *Low-Dose Methotrexate for the Prevention of Atherosclerotic Events.* N Engl J Med, 2019. **380**(8): p. 752-762.

10. Pan, W., et al., *Immunomodulation by Exosomes in Myocardial Infarction.* J Cardiovasc Transl Res, 2019. **12**(1): p. 28-36.

11. Leung, Y.Y., L.L. Yao Hui, and V.B. Kraus, *Colchicine--Update on mechanisms of action and therapeutic uses.* Semin Arthritis Rheum, 2015. **45**(3): p. 341-50.

12. Crittenden, D.B., et al., *Colchicine use is associated with decreased prevalence of myocardial infarction in patients with gout.* J Rheumatol, 2012. **39**(7): p. 1458-64.

13. Langevitz, P., et al., *Prevalence of ischemic heart disease in patients with familial Mediterranean fever.* Isr Med Assoc J, 2001. **3**(1): p. 9-12.

14. Nidorf, S.M., et al., *Low-dose colchicine for secondary prevention of cardiovascular disease.* J Am Coll Cardiol, 2013. **61**(4): p. 404-10.

15. Nidorf, S.M., et al., *The effect of low-dose colchicine in patients with stable coronary artery disease: The LoDoCo2 trial rationale, design, and baseline characteristics.* Am Heart J, 2019. **218**: p. 46-56.

16. Deftereos, S., et al., *Colchicine treatment for the prevention of bare-metal stent restenosis in diabetic patients.* J Am Coll Cardiol, 2013. **61**(16): p. 1679-85.

17. Tardif, J.C., et al., *Efficacy and Safety of Low-Dose Colchicine after Myocardial Infarction.* N Engl J Med, 2019. **381**(26): p. 2497-2505.

18. Bhattacharyya, B., et al., *Anti-mitotic activity of colchicine and the structural basis for its interaction with tubulin.* Med Res Rev, 2008. **28**(1): p. 155-83.

19. Ganguly, A., et al., *Microtubule dynamics control tail retraction in migrating vascular endothelial cells.* Mol Cancer Ther, 2013. **12**(12): p. 2837-46.

20. Paschke, S., et al., *Technical advance: Inhibition of neutrophil chemotaxis by colchicine is modulated through viscoelastic properties of subcellular compartments.* J Leukoc Biol, 2013. **94**(5): p. 1091-6.

21. Peachman, K.K., et al., *Functional microtubules are required for antigen processing by macrophages and dendritic cells.* Immunol Lett, 2004. **95**(1): p. 13-24.

22. Sullivan, D.P. and W.A. Muller, *Neutrophil and monocyte recruitment by PECAM, CD99, and other molecules via the LBRC.* Semin Immunopathol, 2014. **36**(2): p. 193-209.

23. Martinon, F., et al., *Gout-associated uric acid crystals activate the NALP3 inflammasome.* Nature, 2006. **440**(7081): p. 237-41.

24. Pope, R.M. and J. Tschopp, *The role of interleukin-1 and the inflammasome in gout: implications for therapy.* Arthritis Rheum, 2007. **56**(10): p. 3183-8.

25. Cimmino, G., et al., *Colchicine reduces platelet aggregation by modulating cytoskeleton rearrangement via inhibition of cofilin and LIM domain kinase 1.* Vascul Pharmacol, 2018. **111**: p. 62-70.

26. Phinikaridou, A., et al., *A robust rabbit model of human atherosclerosis and atherothrombosis.* J Lipid Res, 2009. **50**(5): p. 787-97.

27. Phinikaridou, A., et al., *In vivo detection of vulnerable atherosclerotic plaque by MRI in a rabbit model.* Circ Cardiovasc Imaging, 2010. **3**(3): p. 323-32.

28. Schroeder, S., et al., *Noninvasive detection and evaluation of atherosclerotic coronary plaques with multislice computed tomography.* J Am Coll Cardiol, 2001. **37**(5): p. 1430-5.

29. Yla-Herttuala, S., et al., *Stabilization of atherosclerotic plaques: an update.* Eur Heart J, 2013. **34**(42): p. 3251-8.

30. Stone, G.W., et al., *A prospective natural-history study of coronary atherosclerosis.* N Engl J Med, 2011. **364**(3): p. 226-35.

31. Naghavi, M., et al., *From vulnerable plaque to vulnerable patient: a call for new definitions and risk assessment strategies: Part II.* Circulation, 2003. **108**(15): p. 1772-8.

32. Arbab-Zadeh, A. and V. Fuster, *The myth of the "vulnerable plaque": transitioning from a focus on individual lesions to atherosclerotic disease burden for coronary artery disease risk assessment.* J Am Coll Cardiol, 2015. **65**(8): p. 846-55.

33. Chiu, B., et al., *Fast plaque burden assessment of the femoral artery using 3D black-blood MRI and automated segmentation.* Med Phys, 2011. **38**(10): p. 5370-84.

34. Kantor, B., et al., *Coronary computed tomography and magnetic resonance imaging.* Curr Probl Cardiol, 2009. **34**(4): p. 145-217.

35. Vaidya, K., et al., *Colchicine Therapy and Plaque Stabilization in Patients With Acute Coronary Syndrome: A CT Coronary Angiography Study.* JACC Cardiovasc Imaging, 2018. **11**(2 Pt 2): p. 305-316.

36. Bauriedel, G., et al., *Colchicine antagonizes the activity of human smooth muscle cells cultivated from arteriosclerotic lesions after atherectomy.* Coron Artery Dis, 1994. **5**(6): p. 531-9.

37. Tatsumi, M., et al., *Fluorodeoxyglucose uptake in the aortic wall at PET/CT: possible finding for active atherosclerosis.* Radiology, 2003. **229**(3): p. 831-7.

38. Tawakol, A., et al., *Noninvasive in vivo measurement of vascular inflammation with F-18 fluorodeoxyglucose positron emission tomography.* J Nucl Cardiol, 2005. **12**(3): p. 294-301.

39. Ishii, H., et al., *Comparison of atorvastatin 5 and 20 mg/d for reducing F-18 fluorodeoxyglucose uptake in atherosclerotic plaques on positron emission tomography/computed tomography: a randomized, investigator-blinded, open-label, 6-month study in Japanese adults scheduled for percutaneous coronary intervention.* Clin Ther, 2010. **32**(14): p. 2337-47.
40. Vucic, E., et al., *Pioglitazone modulates vascular inflammation in atherosclerotic rabbits noninvasive assessment with FDG-PET-CT and dynamic contrast-enhanced MR imaging.* JACC Cardiovasc Imaging, 2011. **4**(10): p. 1100-9.
41. Martinez, G.J., D.S. Celermajer, and S. Patel, *The NLRP3 inflammasome and the emerging role of colchicine to inhibit atherosclerosis-associated inflammation.* Atherosclerosis, 2018. **269**: p. 262-271.
42. Martinez, G.J., et al., *Colchicine Acutely Suppresses Local Cardiac Production of Inflammatory Cytokines in Patients With an Acute Coronary Syndrome.* J Am Heart Assoc, 2015. **4**(8): p. e002128.
43. Yabushita, H., et al., *Characterization of human atherosclerosis by optical coherence tomography.* Circulation, 2002. **106**(13): p. 1640-5.
44. Rodriguez-Granillo, G.A., et al., *[New insights towards catheter-based identification of vulnerable plaque].* Rev Esp Cardiol, 2005. **58**(10): p. 1197-206.
45. Puri, R., et al., *Impact of statins on serial coronary calcification during atheroma progression and regression.* J Am Coll Cardiol, 2015. **65**(13): p. 1273-1282.
46. Kaminiotis, V.V., et al., *Per os colchicine administration in cholesterol fed rabbits: Triglycerides lowering effects without affecting atherosclerosis progress.* Lipids Health Dis, 2017. **16**(1): p. 184.
47. Wojcicki, J., et al., *The effect of colchicine on the development of experimental atherosclerosis in rabbits.* Pol J Pharmacol Pharm, 1986. **38**(4): p. 343-8.

48. Brooks, P.M., D. Burton, and M.J. Forrest, *Crystal-induced inflammation in the rat subcutaneous air-pouch.* Br J Pharmacol, 1987. **90**(2): p. 413-9.

49. Maduri, S. and V.R. Atla, *Formulation of colchicine ointment for the treatment of acute gout.* Singapore Med J, 2012. **53**(11): p. 750-4.

50. Marcovici, I., et al., *Colchicine and post-inflammatory adhesions in a rabbit model: a dose-response study.* Obstet Gynecol, 1993. **82**(2): p. 216-8.

51. Angelidis, C., et al., *Colchicine Pharmacokinetics and Mechanism of Action.* Curr Pharm Des, 2018. **24**(6): p. 659-663.

Tables:

Table 1. Lipid profile and body weight

	Placebo	**Colchicine**	
	Median (IQR)	*Median (IQR)*	*p*
Total Cholesterol			
Pre (mg/dl)	621 (433)	594 (254)	0.88
Post (mg/dl)	728 (405)	667 (450)	0.96
LDL			
Pre (mg/dl)	620 (371)	622 (225)	0.99
Post (mg/dl)	721(487)	662 (423)	0.80
HDL			
Pre (mg/dl)	186 (122)	236 (59)	0.65
Post (mg/dl)	153 (30)	187 (47)	0.13
Triglycerides			
Pre (mg/dl)	97 (20)	55 (61)	0.44
Post (mg/dl)	63 (141)	88 (84)	0.51
Body weight			
Pre (Kg)	3.6 (0.7)	3.6 (0.5)	0.65
Post (kg)	3.5 (0.6)	3.8 (0.4)	0.13

IQR, Interquartile range; Pre, before randomization; Post, at end of the protocol.

Table 2. Main analysis of imaging assessment:

	Placebo (8 rabbits)	Colchicine (8 rabbits)	Colchicine vs Placebo	
	Median (IQR)	*Median (IQR)*	*Difference of the medians (95%CI)*	*p*
Wall volume in MR Imaging				
Pre NWI	0.43 (0.05)	0.42 (0.05)	-0.01 (-0.05 to 0.03)	0.57
Post NWI	0.50 (0.07)	0.48 (0.06)	-0.02 (-0.08 to 0.06)	0.28
Absolute increase	0.06 (0.04)	0.05 (0.04)	-0.01 (-0.05 to 0.02)	0.38
Relative increase, %	14.4 (10.1)	12.0 (10.0)	-2.6 (-11.2 to 4.2)	0.33
^{18}F-FDG uptake in PET/CT Imaging				
Pre meanSUVmax	0.72 (0.23)	0.79 (0.44)	0.04 (-0.14 to 0.34)	0.57
Post meanSUVmax	0.85 (0.19)	0.72 (0.17)	-0.09 (-0.21 to 0.05)	0.13
Absolute increase	0.07 (0.33)	- 0.02 (0.24)	-0.13 (-0.38 to 0.09)	0.20
Relative increase, %	13.7 (48.6)	- 10.9 (32.1)	-16.3 (-55.3 to 7.6)	0.13
High intensity plaque volume in CT Imaging				
Pre Calcium Volume, mm^3	2.34 (5.63)	0.86 (3.61)	-0.62 (-5.49 to 1.59)	0.46
Post Calcium Volume, mm^3	10.38 (36.15)	13.35 (8.03)	1.85 (-9.89 to 29.91)	0.65
Absolute increase, mm^3	10.63 (32.19)	12.08 (13.94)	1.97 (-10.99 to 24.50)	0.96
OCT analysis				
Proportion of lipid plaque	0.93 (0.09)	0.94 (0.08)	0.00 (-0.07 to 0.07)	0.88
Fibrous cap, µm	113.0 (24.5)	119.1 (37.1)	1.24 (-1.41 to 24.20)	0.88
Histology, RAM-11 Stain				
Macrophage infiltration, %	24.0 (31.1)	16.6 (19.2)	-3.0 (-19.2 to 8.6)	0.72
Smooth muscle cell, %	8.7 (5.5)	13.0 (9.9)	2.2 (-1.1 to 9.0)	0.20

IQR, Interquartile Range; NWI, Normalized Wall Index; Pre, before randomization; Post, at end of the protocol; CI95%, 95% Confidence Interval.

Table 3. Subgroup analysis of imaging assessment excluding first quartile of cholesterol levels:

	Placebo (6 rabbits)	Colchicine (6 rabbits)	Colchicine vs Placebo	
	Median (IQR)	*Median (IQR)*	*Difference of the medians (95%CI)*	*p*
Wall volume in MR Imaging				
Pre NWI	0.43 (0.06)	0.42 (0.05)	-0.03 (-0.07 to 0.01)	0.13
Post NWI	0.52 (0.03)	0.47 (0.05)	-0.05 (-0.13 to 0.02)	0.01
Absolute increase	0.07 (0.04)	0.04 (0.04)	-0.03 (-0.07 to 0.01)	0.07
Relative increase, %	16.7 (10.1)	9.0 (10.9)	-7.0 (-16.1 to 1.6)	0.07
^{18}F-FDG uptake in PET/CT Imaging				
Pre meanSUVmax	0.69 (0.26)	0.85 (0.40)	0.19 (0.09 to 0.47)	0.09
Post meanSUVmax	0.88 (0.22)	0.72 (0.14)	-0.13 (-0.22 to 0.06)	0.24
Absolute increase	0.15 (0.35)	- 0.08 (0.28)	-0.25 (-0.52 to 0.01)	0.07
Relative increase, %	35.1 (59.0)	- 4.0 (30.1)	-39.8 (-87.2 to -1.4)	0.04
High intensity plaque volume in CT Imaging				
Pre Calcium Volume, mm^3	2.23 (7.52)	0.86 (4.64)	-0.30 (-6.26 to 3.38)	0.70
Post Calcium Volume, mm^3	25.34 (39.92)	11.37 (7.85)	-14.83 (-36.09 to 7.66)	0.59
Absolute increase, mm^3	18.37 (34.77)	8.66 (12.92)	-8.12 (-34.68 to 7.42)	0.39
OCT analysis				
Proportion of lipid plaque	0.89 (0.11)	0.95 (0.06)	0.04 (-0.04 to 0.10)	0.24
Fibrous cap, µm	112.1 (22.6)	119.1 (37.5)	0.01 (-0.02 to 0.04)	0.70
Histology, RAM-11 Stain				
Macrophage infiltration, %	19.3 (35.7)	16.6 (21.0)	0.44 (-27.7 to 18.0)	0.99
Smooth muscle cell, %	8.1 (4.4)	12.0 (8.2)	1.3 (-1.1 to 9.0)	0.24

IQR, Interquartile Range; NWI, Normalized Wall Index; Pre, before randomization; Post, at end of the protocol; CI95%, 95% Confidence Interval.

Figure Titles and Legends

Figure 1. Study design.

The protocol of the study is shown. Atherosclerosis was induced in the abdominal aorta of 20 rabbits with high-cholesterol diet and balloon endothelial denudation. Rabbits were randomized to receive either colchicine or placebo. All animals underwent magnetic resonance imaging (MRI) and ^{18}F-fluorodeoxyglucose positron emission tomography/computed tomography (^{18}F-FDG PET/CT) prior to randomization and after treatment. Immediately after sacrifice, aortas underwent optical coherence tomography (OCT) and were fixed for histology.

Figure 2. Matching between imaging and histology.

Yellow rectangle marks the region of aorta analyzed in the study. The slices of the different imaging techniques and their correspondence with the histological sections are shown.

Figure 3. Plaque burden

Magnetic Resonance Imaging. On the left, values of normalized wall index per animal in each group and time-point of the study are shown in box plots. Statistical significance of comparisons is presented. On the right, example of typical T1 and T2W spin-echo images illustrating the arterial wall boundaries segmentation of a slice of the abdominal aorta. Pre, before randomization; Post, at end of the protocol.

Figure 4. Inflammation.

A, ^{18}F-FDG PET/CT Imaging. On the left, ^{18}F-FDG uptake values per animal in each group and time-point of the study are shown in box plots. Statistical significance of comparisons is presented. In the middle, in vivo combined PET/computed tomography (CT) coronal view of the abdominal aorta illustrating the ^{18}F-FDG uptake. In the rightmost, axial views of the corresponding slice indicated with a dotted line in the coronal view of the PET/CT image are showed: top panel, increased ^{18}F-FDG uptake; bottom panel, the corresponding T1-weighted magnetic resonance image illustrates aortic atherosclerosis lesion development. Pre, before randomization; Post, at end of the protocol. B, Macrophage immunostaining. Values of percentage of total vessel wall area occupied by macrophages per animal in each group are shown in box plot. Statistical significance of comparisons is presented. On the right, an axial slices stained with RAM-11 antibody. C, Interleukin 6. Values IL-6 per animal in each group at the end of protocol are shown in box plot

Figure 5. Plaque typology.

A, Optical coherence tomography. On the left, values of proportion of lipid plaque per animal in each group are shown in box plot. Statistical significance of comparisons is presented. On the right, an axial slice of a lipid plaque illustrating the plaque typology assessment. B, Computed tomography. On the left, values of high CT intensity plaque volume per animal in each group and time-point of the study are shown in box plot. Statistical significance of comparisons is presented. On the right, coronal view of abdominal aorta showing high signal spots in the CT image along the vessel. In the rightmost panel, histological staining confirmed the ability of CT to detect aortic calcifications in this animal model. The yellow box delimits the 8-cm of abdominal aorta assessed by this study. Pre, before randomization; Post, at end of the protocol.

Figure 6. Inflammatory activity in the subgroup analysis excluding lower cholesterol animals.

On the left, meanSUVmax per animal in each group and time-point of the study are shown in box plot. Statistical significance of comparisons is presented. On the right, relative increase of meanSUVmax per animal in each group is shown in a box plot. Pre, before randomization; Post, at end of the protocol.

Figure 1

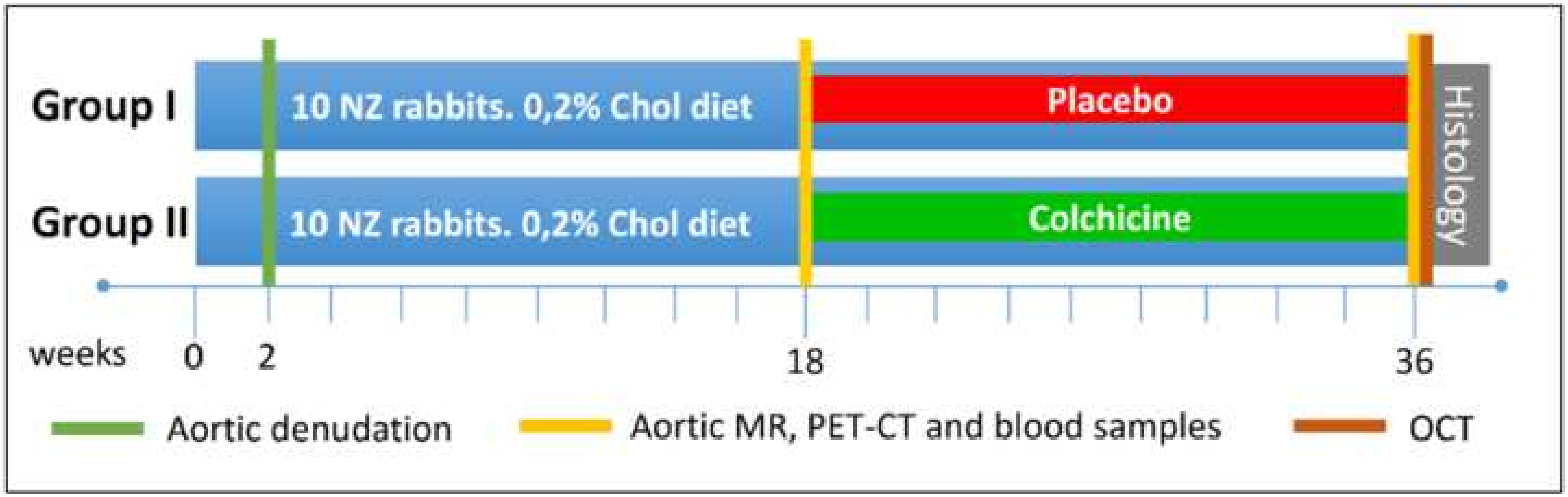

Group I
10 NZ rabbits. 0,2% Chol diet
Placebo
Group II
10 NZ rabbits. 0,2% Chol diet
Colchicine
Histology
weeks
0
2
18
36
Aortic denudation
Aortic MR, PET-CT and blood samples
OCT

Figure 2

Click here to access/download;Figure;Figure 2.tif

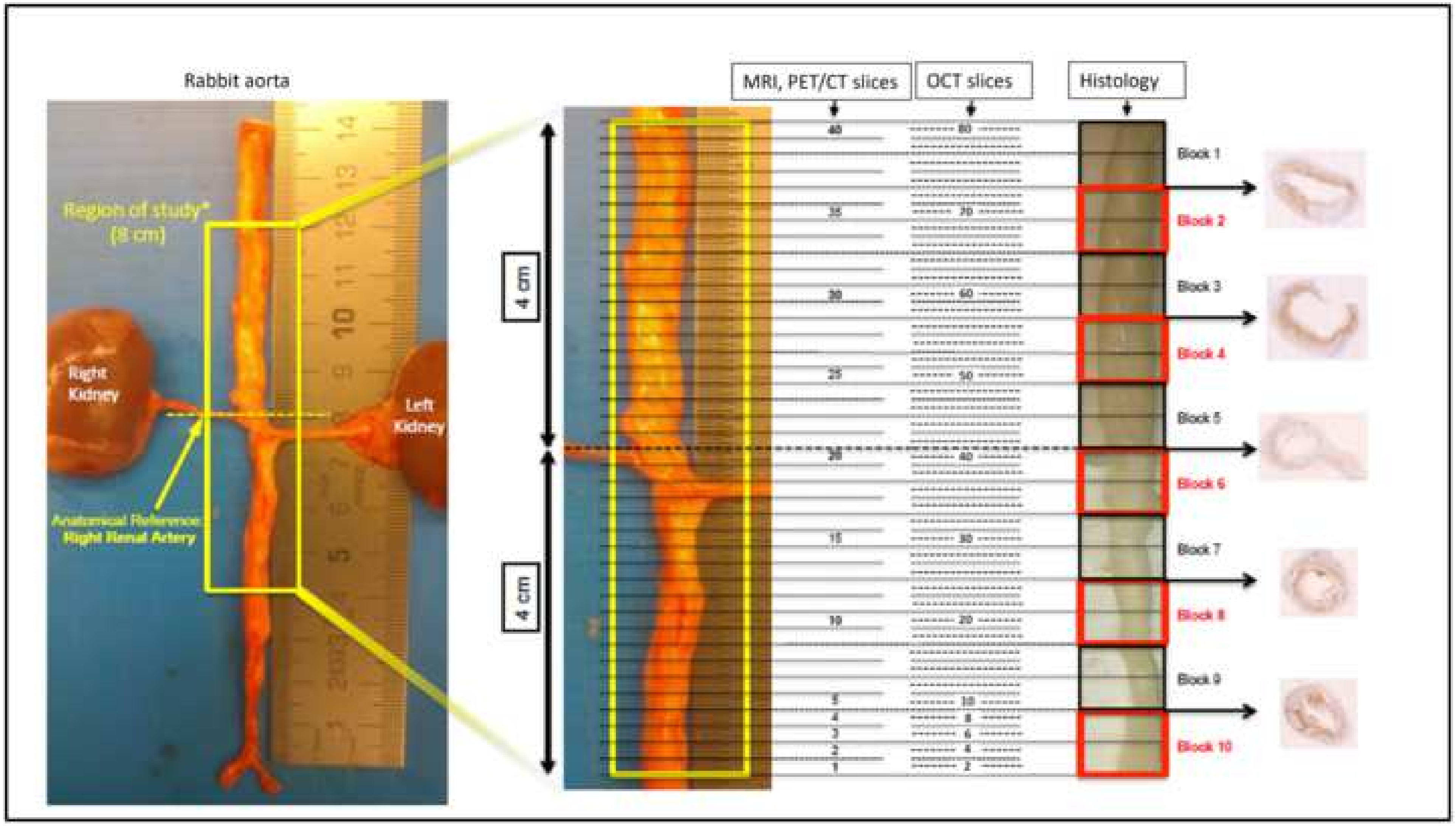

Figure 3

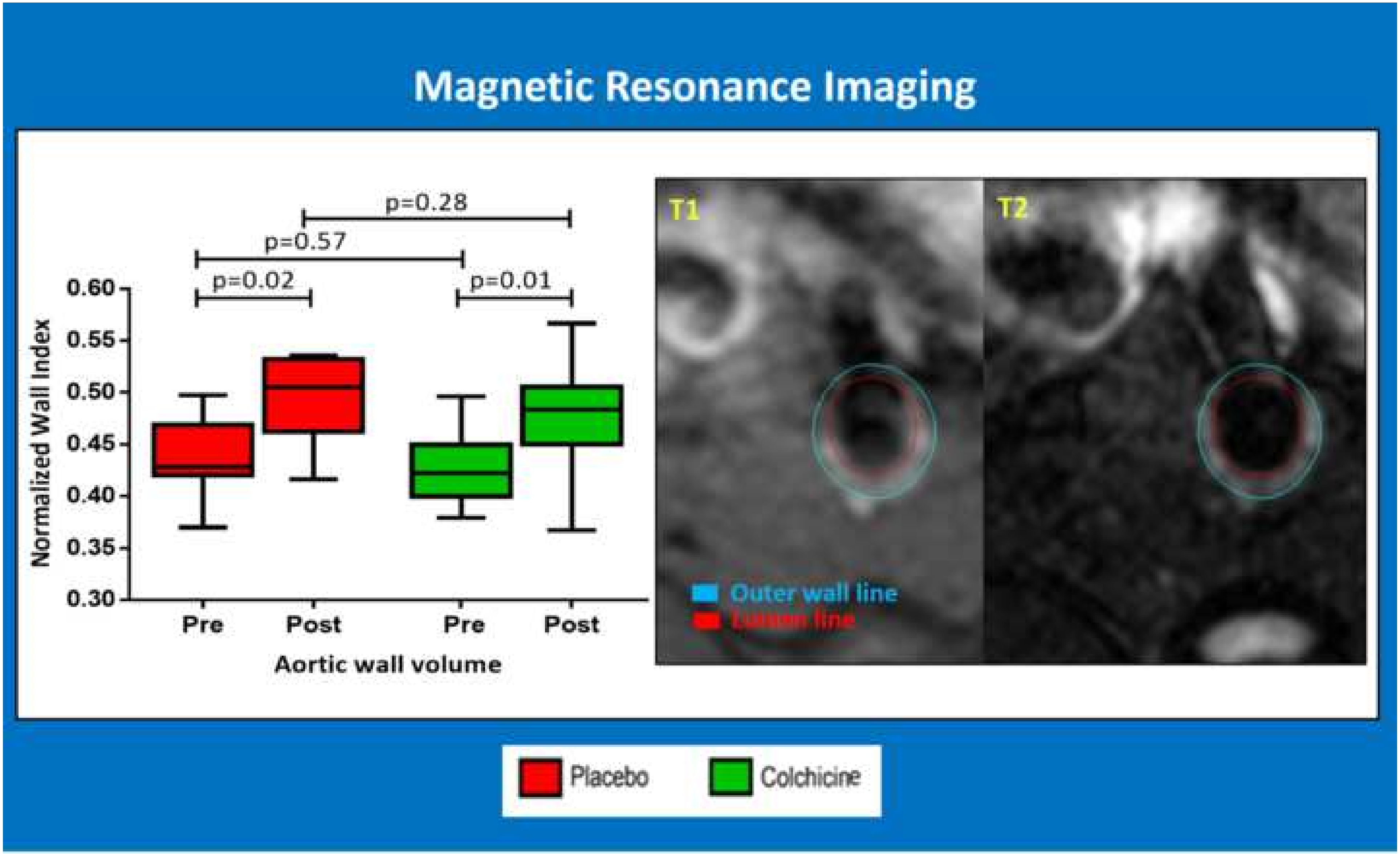

Magnetic Resonance Imaging
p=0.28
p=0.57
p=0.02
p=0.01
Normalized Wall Index
0.60
0.55
0.50
0.45
0.40
0.35
0.30
Pre
Post
Pre
Post
Aortic wall volume
T1
T2
Outer wall line
Lumen line
Placebo
Colchicine

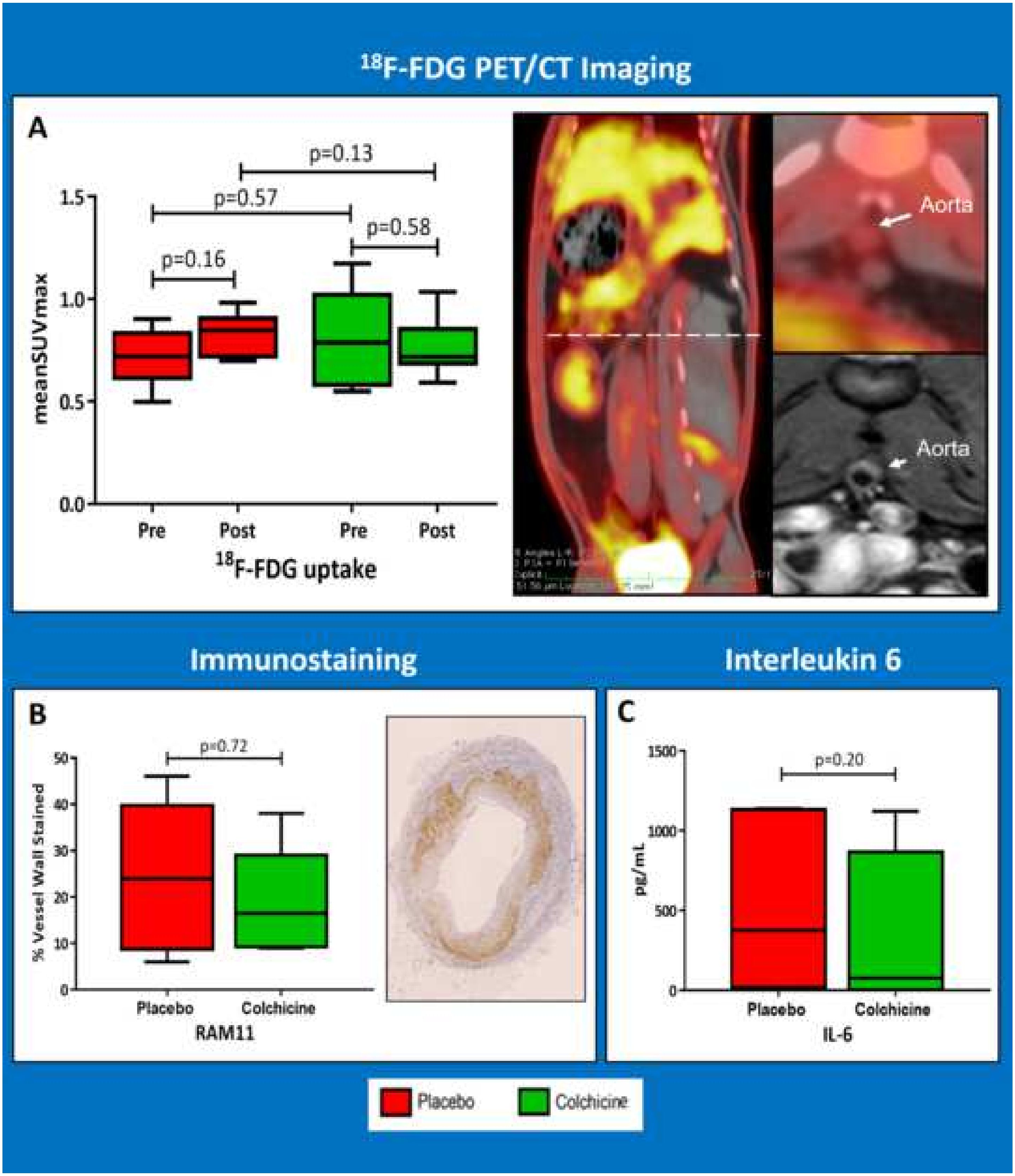
18F-FDG PET/CT Imaging
A
meanSUVmax
1.5
1.0
0.5
0.0
p=0.13
p=0.57
p=0.58
p=0.16
Pre
Post
Pre
Post
18F-FDG uptake
Aorta
Aorta
Immunostaining
Interleukin 6
B
% Vessel Wall Stained
50
40
30
20
10
0
p=0.72
Placebo
Colchicine
RAM11
C
pg/mL
1500
1000
500
0
p=0.20
Placebo
Colchicine
IL-6
Placebo
Colchicine

Figure 5

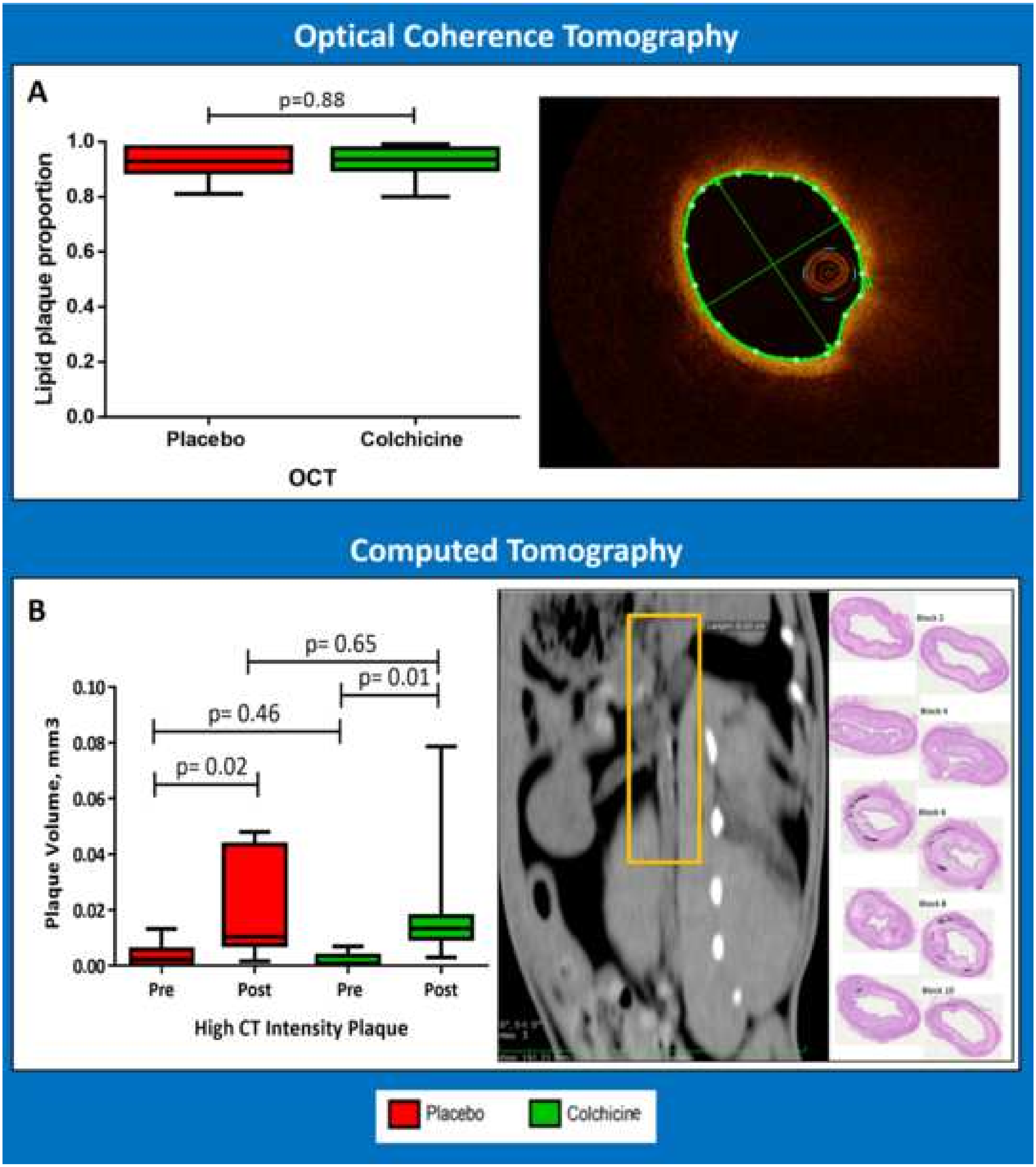
Optical Coherence Tomography
A
p=0.88
Lipid plaque proportion
1.0
0.8
0.6
0.4
0.2
0.0
Placebo
Colchicine
OCT
Computed Tomography
B
p= 0.65
p= 0.01
p= 0.46
p= 0.02
Plaque Volume, mm3
0.10
0.08
0.06
0.04
0.02
0.00
Pre
Post
Pre
Post
High CT Intensity Plaque
Placebo
Colchicine

Figure 6

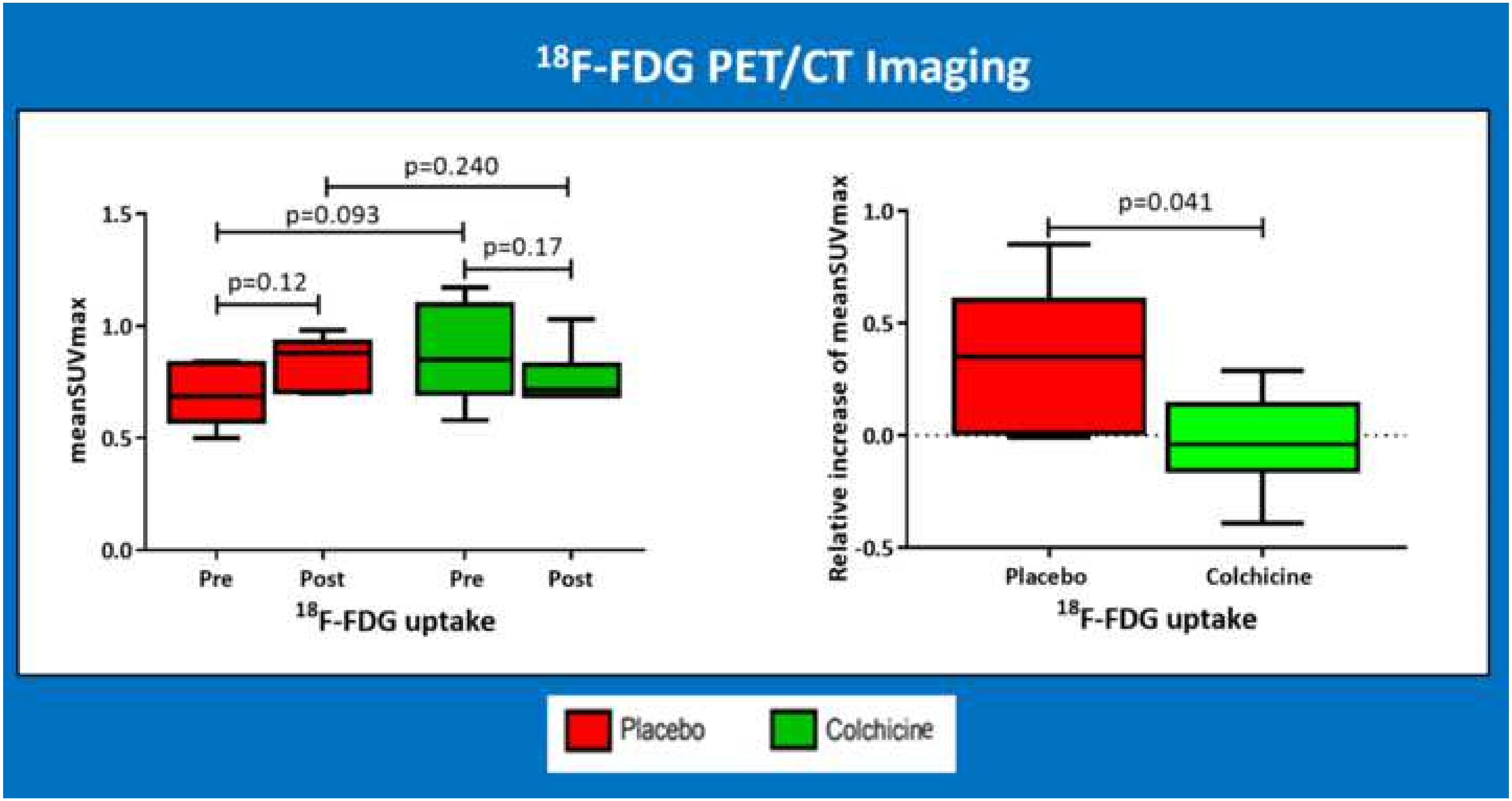

18F-FDG PET/CT Imaging
p=0.240
p=0.093
p=0.17
p=0.12
1.5
1.0
0.5
0.0
meanSUVmax
Pre
Post
Pre
Post
18F-FDG uptake
p=0.041
1.0
0.5
0.0
-0.5
Relative increase of meanSUVmax
Placebo
Colchicine
18F-FDG uptake
Placebo
Colchicine

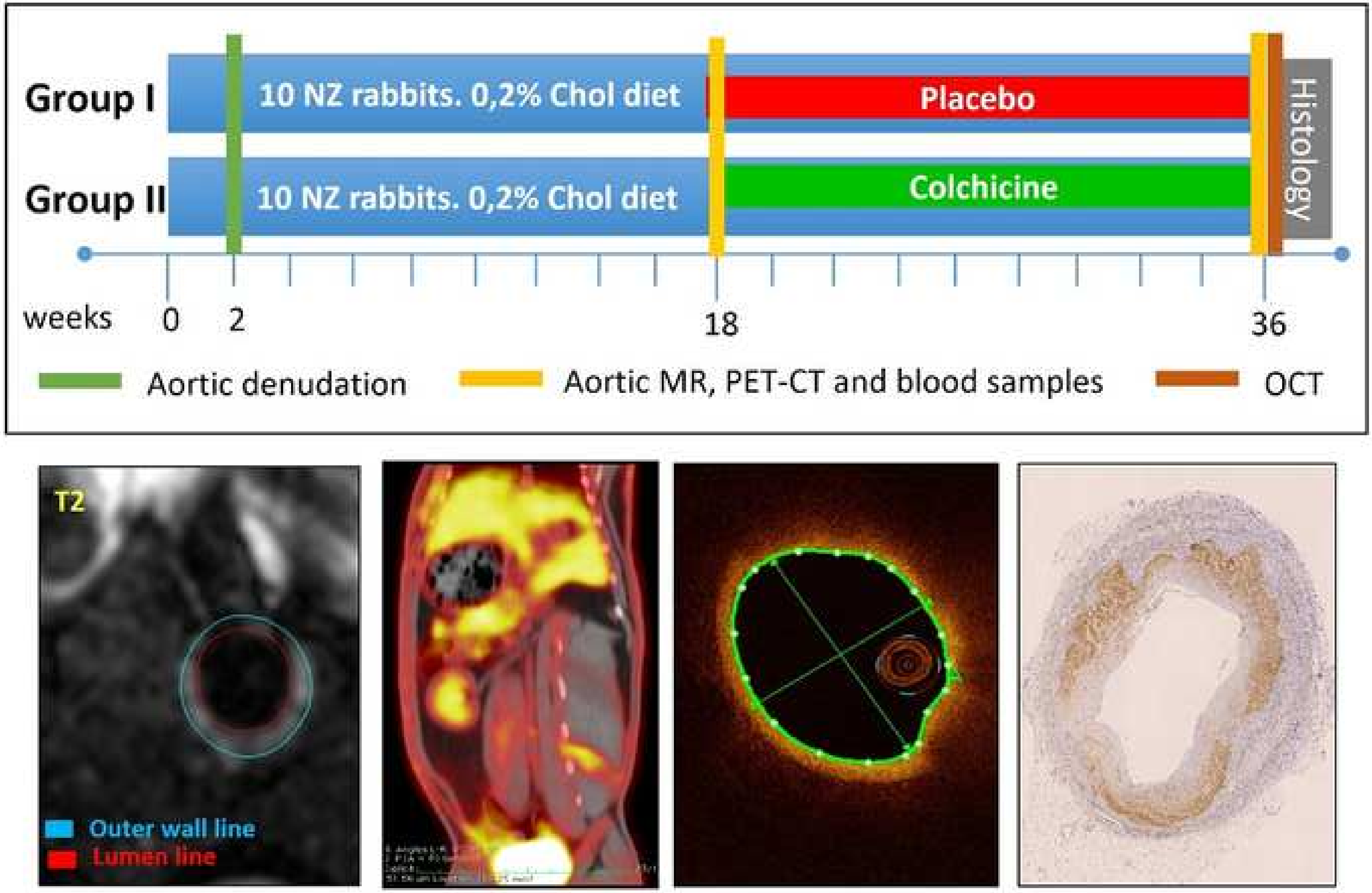

Multi-imaging assessment suggests that colchicine, *in vivo*, could reduce vulnerability state of coronary artery disease by a reduction of inflammatory activity and plaque burden.